16.4 HODOGRAPH VARIABILITY WITHIN ANALYTICALLY MODELED BAROCLINIC WAVES

Peter C. Banacos *
NOAA/Storm Prediction Center
Norman, Oklahoma 73069

Howard B. Bluestein
University of Oklahoma
Norman, Oklahoma 73019

1. INTRODUCTION

Observational (Maddox 1976; Bluestein and Jain, 1985) and numerical (Weisman and Klemp, 1984) studies have shown that relatively minor changes in the vertical shear profile can have a strong modulating influence on the "mode" of deep moist convection (i.e. the favored organizational structure of convective storms or systems) in conjunction with other physical factors (the most prominent being the magnitude and vertical distribution of instability, and the nature and magnitude of the vertical motion mechanism(s)). These studies have not explored how synoptic-scale baroclinic wave structures modulate the wind field locally, which could change the organization of mesoscale precipitation. Owing to the frequent connection between severe convection and synoptic-scale troughs, we have employed a relatively simple analytic model herein to associate better the local shear profile with parameters that describe the character of the synoptic-scale baroclinic wave. A hodograph climatology, developed relative to synoptic-scale cyclones and anticyclones locations over a 37 year period (Bluestein and Banacos, 2002), serves as a guide in assessing the analytically generated model hodographs.

2. MODEL DESCRIPTION AND METHODOLOGY

An analytic model developed by Sanders (1971), which has exact solutions for a quasi-geostrophic (QG) atmosphere without friction, was used to vary systematically the configuration of the synoptic-scale baroclinic waves. From a specification of the geopotential field at 1000mb, subsequent integration and use of the hydrostatic equation yields the following three-dimensional geopotential and temperature field equations (see Sanders, 1971 and Bluestein, 1993 for details):

$$\Phi(x,y,p)=\Phi_m(p)+\hat{\Phi}_o\cos\frac{2\pi}{L}(x+\lambda)\cos\frac{2\pi y}{L}+ R\left(ay+\hat{T}\cos\frac{2\pi x}{L}\cos\frac{2\pi y}{L}\right)\left[\ln\frac{p}{1000}+\frac{\alpha}{2}\left(\ln\frac{p}{1000}\right)^2\right] \quad (1)$$

$$T(x,y,p)=T_m(p)-\left(1-\alpha\ln\frac{1000}{p}\right)\left(ay+\hat{T}\cos\frac{2\pi x}{L}\cos\frac{2\pi y}{L}\right) \quad (2)$$

where Φ is geopotential, Φ_m is level mean geopotential, $\hat{\Phi}_o$ is the surface geopotential perturbation, $\hat{T}$ is the temperature perturbation, T is temperature, T_m is level mean temperature, L is the system wavelength, R is the gas constant for dry air, a is the meridional temperature gradient, α is a parameter controlling tropopause height (set at 250mb), and λ represents the phase lag of the 1000mb geopotential field relative to the temperature field. The x and y axes are directed eastward and northward, respectively; p is pressure expressed in millibars. An f-plane was assumed at 40° N latitude with the model's lowest level at 1000mb set as the Earth's surface. To generate hodographs, equations (1) and (2) were used with equations for the geostrophic ($\mathbf{v}_g$) and ageostrophic ($\mathbf{v}_a$) wind, in order to compute the total horizontal wind ($\mathbf{v}$).

Table 1. Parameter values used in individual model runs

variable (units)	*"control" value*	*parameter range*	*interval*
a (K/1000 km)	*10*	*2.5 –> 22.5*	*2.5*
L (km)	*3500*	*2500 –> 4500*	*250*
λ (km)	*L/4*	*0 –> L/2*	*L/16*
$\hat{T}$ (K)	*10*	*0 –> 20*	*2.5*
$\hat{\Phi}_o$ (m^2s^{-2})	*1020*	*0 –> 1020*	*127.5*

We are interested primarily in the effects of five variables controlling the baroclinic wave structure: (1) meridional temperature gradient, (2) system wavelength, (3) phase lag, (4) magnitude of the temperature perturbation, and (5) magnitude of the surface height perturbation. Each were modulated independently from the others and from a "control" simulation, over a parameter space consistent with values commonly observed in mid-latitude pressure systems. Nine values of each parameter (Table 1) were analyzed at three points located one-sixteenth of a wavelength (equivalent to 219km for the control run) northeast, east, and southeast of the surface cyclone center for the control and each parameter modulation, at a frozen point in time (we chose locations downstream of cyclones since that is where deep convective storms tend to be most common and intense). This procedure yielded 138 individual hodographs valid for a wide spectrum of baroclinic wave intensities and configurations.

3. WIND FIELD AND HODOGRAPH ANALYSIS

3a. aspects of the "control" simulation

The "control" simulation represents moderately intense, westward sloping baroclinic waves configured such that the temperature field lags the 1000mb height

* Corresponding author address: Peter C. Banacos, Storm Prediction Center, 1313 Halley Circle, Norman, OK 73069; e-mail: peter.banacos@noaa.gov

field by one-quarter wavelength (Fig. 1). This represents the most unstable phase lag consistent with baroclinic instability theory, and leads to height tendency fields indicative of a rapidly amplifying/intensifying wave at both 1000 and 500mb. A relatively strong baroclinic zone exists to the northeast and southwest of the surface low. The magnitude of the quasi-horizontal temperature gradient decreases with height, however, the isotherm *orientation* does not change. From the thermal wind relationship, this implies vertical shear in $\mathbf{v}_g$ must be unidirectional in the model. In nature, straight hodographs are observed in the mean to a first-order approximation away from the tropopause and planetary boundary layer (PBL) (e.g., Bluestein and Banacos, 2002, Fig. 5). Minimal change in isotherm orientation with height is also often observed within frontogenetic deformation zones where narrow banded precipitation areas are sometimes found, however, there is not necessarily a physical constraint on the vertical parallelism of the horizontal temperature gradient. Additionally, since friction is not included in the model, curvature in the total wind hodograph must be derived from QG $\mathbf{v}_a$:

$$\mathbf{v}_a = \frac{1}{f}\mathbf{k}\times\frac{D\mathbf{v}}{Dt} = \frac{1}{f}\mathbf{k}\times\left[\frac{\partial \mathbf{v}_g}{\partial t} + (\mathbf{v}_g \bullet \nabla_p)\mathbf{v}_g\right] \qquad (3)$$

where the first and second terms in brackets represent the isallohypsic (Fig. 1c and d) and inertial-advective (Fig. 2) components, respectively. As can be seen by comparing Figs. 1 and 2, it is common for the isallohypsic wind, which points "down" the gradient of height tendency, to act opposite of the inertial-advective wind, directed generally perpendicular and to the left of the horizontal parcel acceleration. Thus, it can be extremely difficult to qualitatively assess the resultant magnitude of $\mathbf{v}_a$. The inertial-advective wind at 1000mb (not shown) is smaller than at higher elevations owing to generally smaller values of **v** and del **v**. The isallohypsic contribution to $\mathbf{v}_a$ does not vary appreciably with respect to height in the control simulation; however, its magnitude relative to the inertial-advective wind is larger at low-levels. At the surface, the geopotential tendency field is dominated by the effects of warm advection decreasing with height northeast of the surface cyclone, where height falls (and deep-layer vertical motion) are maximized. In the mid-troposphere, the height falls are largest east of the surface low, owing to the dominant effect of vorticity advection east of the 500mb trough, and the reduction of temperature advection with decreasing pressure in the model.

This analysis aids in explaining the $\mathbf{v}_g$, $\mathbf{v}_a$, and **v**

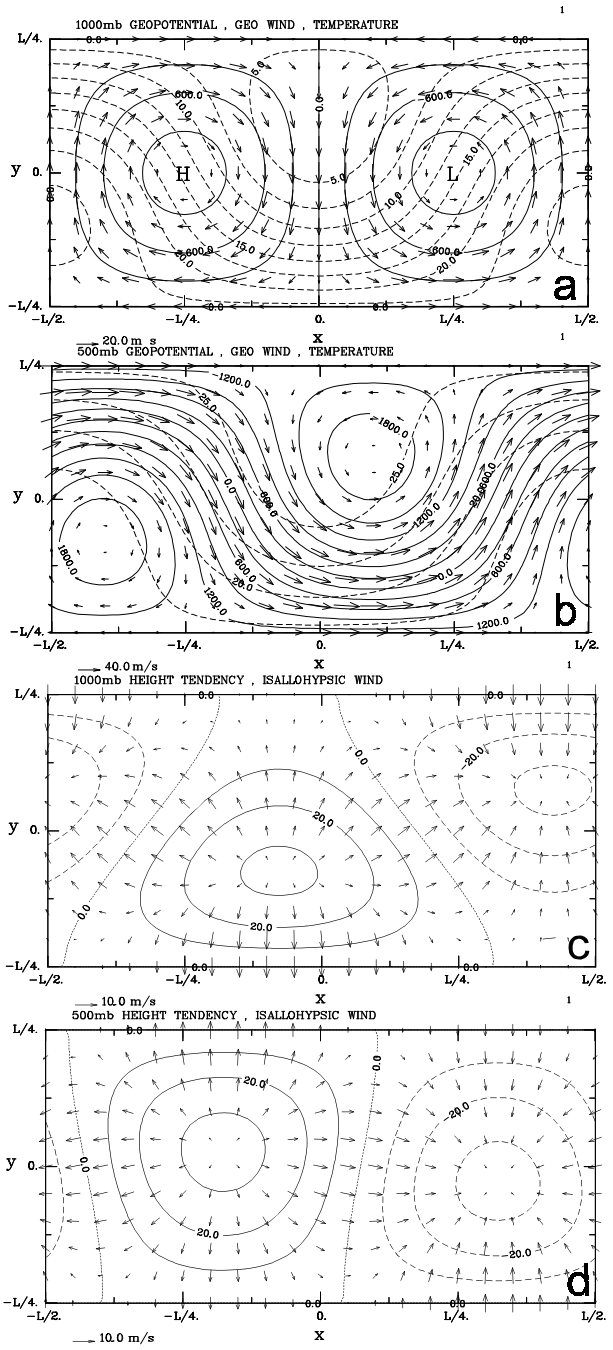

Figure 1. Control configuration. The 1000mb (a) and 500mb (b) geopotential (solid lines) and temperature fields (dashed lines) and geostrophic wind. The 1000mb (c) and 500mb (d) height tendency field (negative values dashed) and isallohypsic wind.

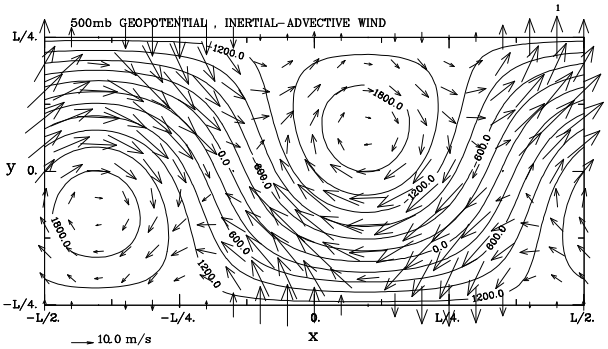

Figure 2. Control configuration. The 500mb geopotential field and inertial-advective wind.

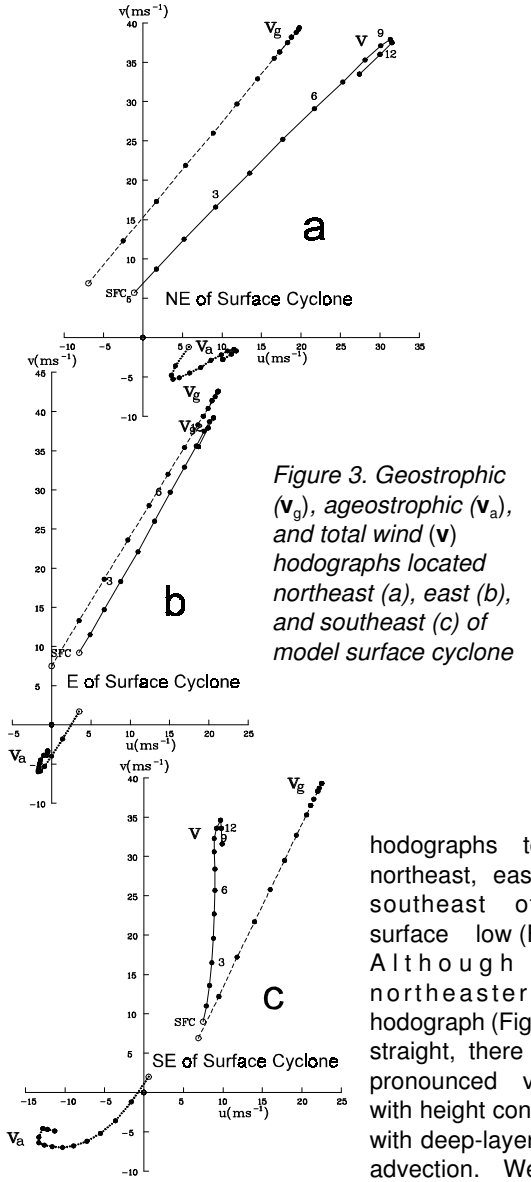

*Figure 3. Geostrophic (**v**$_g$), ageostrophic (**v**$_a$), and total wind (**v**) hodographs located northeast (a), east (b), and southeast (c) of model surface cyclone*

hodographs to the northeast, east, and southeast of the surface low (Fig. 3). Although the northeastern **v**$_g$ hodograph (Fig. 3a) is straight, there is still pronounced veering with height consistent with deep-layer warm advection. We see that the **v**$_g$ shear weakens gradually with height, and that the hodograph "folds" over onto itself at the tropopause as the del T vector reverses sign. A comparison of Fig. 1c with Fig. 1d shows **v**$_a$ veers in the low-levels, largely following the movement of the negative height tendency center. At 3km AGL, **v**$_a$ backs with height until the tropopause, increasingly affected by the northeastward pointing inertial-advective wind downstream of the trough/ridge inflection point (Fig. 2). The reversal in temperature gradient above the tropopause yields an anticyclonic turning hodograph between 10-13km AGL, and leads directly to the same turning in the total wind hodograph. This turning at the tropopause was observed in composite mean hodographs in Bluestein and Banacos (2002), but was generally broader, suggesting a more gradual change in wind direction. This turning may be attributable to curvature in the **v**$_g$ hodograph that does not occur in the model, or partly due to the smearing effect of averaging rawinsonde winds across varying tropopause heights in the observational composites. Below the tropopause, the model hodograph compares reasonably well with observation, with the obvious exception of the absence of hodograph curvature in the PBL.

To the east of the cyclone (Fig. 3b), the **v**$_g$ and **v** hodographs are more backed aloft owing to the more meridional upper flow, while exhibiting less veering due to decreased warm temperature advection in the area. The **v**$_a$ component is small in comparison to **v**$_g$ and smaller than northeast of the cyclone; however, it also more directly opposes **v**$_g$, owing to cyclonic flow aloft and a dominant inertial-advective contribution. Of the three hodographs, the largest magnitude of **v**$_a$ is found southeast of the cyclone (Fig. 3c) (approximately one-third of |**v**$_g$| at 10km AGL), beneath the "core" of strongest upper-flow and strong cyclonic curvature to the flow.

3b. baroclinic wave parameter modulations

Space limitations preclude a complete analysis of each case. Shear values are summarized in Table 2 east of the surface cyclone for two parameter settings, so that the reader may get a sense for the incurred variability in the wind profile. Since curvature in the **v** hodograph can only arise from **v**$_a$, it is interesting to note the parameters that lead most strongly to large **v**$_a$ shear relative to **v**$_g$ shear. Although curvature in **v**$_a$ will not necessarily be manifest directly east of the cyclone (depending on the exact way the isallohypsic and inertial-advective components are juxtaposed to create **v**$_a$) when the |**v**$_a$|/|**v**$_g$| ratio is large, curvature that *may* exist in the **v**$_a$ hodograph will be more strongly reflected in the **v** hodograph which can have important consequences (e.g., on tornado potential). In particular, variation of the 0-6km |**v**$_a$|/|**v**$_g$| shear ratio occurred most dramatically with changes in (in descending order) the phase lag, wavelength, and magnitude of the temperature perturbation, but only very minimally with changes in meridional temperature gradient or the magnitude of the surface geopotential perturbation.

As system wavelength is lowered, the 0-6km |**v**$_a$|/|**v**$_g$| shear ratio increases despite the effective increase in **v**$_g$ shear owing to an increased height gradient as *L* shortens. The inertial-advective wind is strongly influenced by the increased curvature in the height pattern and contributes to this effect. At *L*=2500km, the magnitude of height fall centers are increased compared to the control run northeastward of the cyclone at 1000mb by 25% due to enhanced differential warm advection, and by 57% east of the cyclone at 500mb due to increased cyclonic vorticity advection. So, the isallohypsic contribution is also increased. Therefore, shorter wavelength, and often relatively fast moving baroclinc troughs, have the potential to induce large ageostrophic influences on the total wind field, provided QG theory still applies given the small value of wavelength.

Modification of perturbation temperature gradient increases the height gradient in the mid-troposphere,

Table 2. Parameter modulations *L*/16 EAST of surface cyclone

	Parameter value compared to control value	$\mathbf{v}_a$ shear 0-6km (m/s)	$\mathbf{v}_g$ shear 0-6km (m/s)	$\mathbf{v}$ shear 0-6km (m/s)	$\lvert\mathbf{v}_a\rvert$ / $\lvert\mathbf{v}_g\rvert$ 0-6km shear ratio	storm motion 20R/85 (m/s)	0-3 km SRH m^2s^{-2}
Control	n/a	35°/ 9	211°/ 33	210°/ 24	0.280	230°/ 20	147
a	20 K/1000km	55°/ 13	230°/ 44	228°/ 31	0.297	248°/ 26	240
	1 K/1000km	9°/ 8	189°/ 28	189°/ 21	0.269	209°/ 18	111
L	4000 km	38°/ 7	215°/ 30	213°/ 23	0.230	233°/ 19	154
	2500 km	27°/ 19	203°/ 43	201°/ 24	0.437	221°/ 20	79
λ	*3L*/8	24°/ 24	211°/ 33	229°/ 10	0.722	249°/ 8	65
	L/8	75°/ 4	218°/ 27	213°/ 25	0.130	233°/ 21	17
$\hat{T}$	15 K	32°/ 8	202°/ 45	200°/ 37	0.172	220°/ 32	266
	5 K	51°/ 8	230°/ 22	230°/ 14	0.372	250°/ 12	88
$\hat{\Phi}_o$	510 m^2s^{-2}	69°/ 2	211°/ 33	209°/ 31	0.052	229°/ 27	186
	0 m^2s^{-2}	200°/ 7	211°/ 33	209°/ 39	0.201	229°/ 33	182

acting to increase the 0-6km $|\mathbf{v}_a|/|\mathbf{v}_g|$ shear ratio primarily through a positive inertial-advective response to greater curvature in the height field. Since $\mathbf{v}_a$ in this case is relatively straight and points opposite to $\mathbf{v}_g$, the dynamic consequences are likely less than they would be for wavelength modulation where both isallohypsic and inertial-advective components undergo increases.

Modulation of λ was the most complicated to analyze. When the westward tilt of the cyclone is small, low-level temperature advection is decreased in the model (becomes zero when the system is "vertically stacked"), and shifts the height falls southward toward the cyclone warm sector. The quasi-horizontal height gradient is increased aloft for these configurations, increasing the southward to southwestward directed inertial-advective wind. The low-level curvature was most enhanced between 3*L*/8 and 5*L*/16 both east and northeast of the surface cyclone center, due to these effects.

Changes in surface geopotential perturbation were found to be relatively unimportant since the magnitude of the temperature perturbation describes the geopotential distribution aloft which largely controls the deep-layer shear. An increase (decrease) in meridional temperature gradient caused the deep-layer shear to be more zonal (meridional); however, the magnitude of the shear was not strongly affected. It was noted that decreasing (increasing) *a* results in a dramatic decrease (increase) in the magnitude of height tendency. Cyclogenesis is not sustained at low values of *a*, which would soon weaken the system and, correspondingly, $\mathbf{v}_a$ shear values.

Storm relative helicity (SRH) values in the 0-3km AGL layer varied by 200 m^2s^{-2}, but the low to moderate magnitudes indicate the importance of friction and sub-synoptic scale features in enhancing SRH. Somewhat higher SRH values (up to 325 m^2s^{-2}) are found northeast of the surface low (not shown) owing to very strong low-level warm advection in the frontal zone and veering in the $\mathbf{v}_a$ hodograph. However, this is still much less than values commonly observed along warm frontal zones northeast of lows. Although hodograph curvature is generally higher in this area, the thermal stratification often makes it difficult to generate surface-based potential instability due to large-scale ascent, widespread stratiform clouds, and precipitation common to the warm frontal zone.

4. DISCUSSION AND FUTURE WORK

We focused here on five synoptic-scale parameters specific to Sanders' model, which caused appreciable variability in the wind shears locally. These results speak to the difficulty of convective mode forecasting, even when the problem is simplified rather substantially. In particular, the complex interrelationship between temperature advection, frictional, and ageostrophic forcing in the PBL is difficult to incorporate analytically, and was beyond the scope of this research. Use of a numerical model to do the same type of experiments would be needed to consider more accurately some effects, particularly those in the PBL.

There are, of course, an infinite number of synoptic-scale baroclinic wave configurations that are possible in the model. An observational study of $\mathbf{v}_g$ and $\mathbf{v}_a$ hodographs, which goes beyond the climatology of Bluestein and Banacos (2002), classified with specific regard to measured large-scale parameters (such as those used in Sanders' model) would be useful to better understand the synoptic-scale influences on the wind field in close proximity to where convective storms develop.

5. ACKNOWLEDGMENTS

Portions of this work were supported by NSF Grant ATM-9612674 and the School of Meteorology at OU.

REFERENCES

Bluestein, H. B., and P. C. Banacos, 2002: The vertical profile of wind and temperature in cyclones and anticyclones over the eastern two-thirds of the United States: A climatology. *Mon. Wea. Rev.*, **130**, 477–506.

_____, 1993: *Observations and Theory of Weather Systems.* Vol. II. *Synoptic-Dynamic Meteorology in Midlatitudes,* Oxford University Press, 594 pp.

_____, and M. H. Jain, 1985: Formation of mesoscale lines of precipitation: Severe squall lines in Oklahoma during the spring. *J. Atmos. Sci.*, **42**, 1711-1732.

Maddox, R. A., 1976: An evaluation of tornado proximity wind and stability data. *Mon. Wea. Rev.*, **104**, 133-142.

Sanders, F., 1971: Analytic solutions of the non-linear omega and vorticity equation for a structurally simple model of disturbances in the baroclinic westerlies. *Mon. Wea. Rev.*, **99**, 393-407.

Weisman, M. L., and J. B. Klemp, 1984: The structure and classification of numerically simulated convective storms in directionally varying wind shears. *Mon. Wea. Rev.*, **112**, 2479-2498.